dent of pH, adsorption above the CMC is in the higher density form of cylinders. The curvature of the interfacial aggregate thus appears to be a compromise between the free curvature defined by intermolecular interactions and constraints imposed by molecule-surface interactions.

Further study of interfacial surfactant aggregation may lead not only to an enhanced understanding of self-assembly but also to applications in materials science. Interfacial aggregates could, for example, serve as a basis for surface patterning on the nanometer scale, complementing recent patterning strategies on the submicrometer scale (*29*). "Fixing" the liquid-crystalline aggregates could be accomplished by ultraviolet polymerization of modified tailgroups, electroless metal deposition (*30*), or polymerization of certain inorganic counterions (*31*) such as silicates.

REFERENCES AND NOTES

1. J. N. Israelachvili, *Intermolecular and Surface Forces* (Academic Press, London, ed. 2, 1992), pp. 341–385.
2. W. Helfrich, *J. Phys. Condensed Matter* **6**, A79 (1994).
3. S. M. Gruner, *J. Phys. Chem.* **93**, 7562 (1989).
4. A. M. Gaudin and D. W. Fuerstenau, *Trans. Am. Inst. Min. Metall. Pet. Eng.* **202**, 958 (1955); D. W. Fuerstenau, *J. Phys. Chem.* **60**, 981 (1956); J. J. Kipling, *Adsorption from Solution of Non-Electrolytes* (Academic Press, London, 1965).
5. R. M. Pashley and J. N. Israelachvili, *Colloids Surf.* **2**, 169 (1981); R. M. Pashley, P. M. McGuiggan, R. G. Horn, B. W. Ninham, *J. Colloid Interface Sci.* **126**, 569 (1988); P. Kekicheff, H. K. Christenson, B. W. Ninham, *Colloids Surf.* **40**, 31 (1989); J. L. Parker, *Prog. Surf. Sci.* **47**, 205 (1994).
6. P. Levitz, H. Van Damme, D. Keravis, *J. Phys. Chem.* **88**, 2228 (1984).
7. D. C. McDermott, J. McCarney, R. K. Thomas, A. R. Rennie, *J. Colloid Interface Sci.* **162**, 304 (1994).
8. G. Binnig, C. F. Quate, Ch. Gerber, *Phys. Rev. Lett.* **56**, 930 (1986).
9. F. Reiss-Husson and V. Luzzati, *J. Phys. Chem.* **68**, 3504 (1964).
10. T. J. Senden, C. J. Drummond, P. Kekicheff, *Langmuir* **10**, 358 (1994).
11. S. Manne, J. P. Cleveland, H. E. Gaub, G. D. Stucky, P. K. Hansma, *ibid.*, p. 4409.
12. We used a commercial atomic force microscope (Digital Instruments, Santa Barbara, CA) and cantilevers (Ultralevers; Park Scientific Instruments, Sunnyvale, CA) cleaned by exposure to ultraviolet light for 15 to 60 min. Typical imaging times were 30 to 60 s, and imaging forces were ~1 nN. Samples were immersed in surfactant solution long enough to minimize thermal drift of the cantilever (15 to 120 min); mica immersed for several days showed no difference in the aggregate structure, indicating that the adsorbate reaches equilibrium configuration within a few minutes. Surfactants were purchased from Fluka (Buchs, Switzerland) (>98% pure), and solutions were prepared in Millipore water. Highly oriented pyrolytic graphite (Digital Instruments), mica, and the MoS_2 crystal were exposed to surfactant solution within 3 min of cleavage. Silica samples [thermally grown oxide on a Si (100) wafer (Wacker, Burghausen, Germany)] were cleaned and stored as described (*13*) and were mounted and exposed to surfactant solution within 20 min of removal from the storage oven. All images shown are unfiltered except for slope removal along scan lines. Typical force versus distance curves in 7 mM C_{14}TAB solution showed a long-range repulsion that varied exponentially (*32*) with a measured decay length of 2.8 ± 0.3 nm, comparing favorably to a theoretical double-layer decay length of 2.9 nm [calculated from (*21*), assuming that micelles are composed of ~70 molecules of which 25% are dissociated]. The short-range repulsion (at separations <~6 nm) was usually steeper, indicating steric or entropic effects such as hydration forces, counterion confinement, and adsorbate protrusion forces.
13. R. W. Tillmann, M. Radmacher, H. E. Gaub, *Appl. Phys. Lett.* **60**, 3111 (1992).
14. B. H. Bijsterbosch, *J. Colloid Interface Sci.* **47**, 186 (1974).
15. M. A. Yeskie and J. H. Harwell, *J. Phys. Chem.* **92**, 2346 (1988).
16. R. K. Iler, *The Chemistry of Silica* (Wiley, New York, 1979), pp. 680–686.
17. M. W. Rutland and J. L. Parker, *Langmuir* **10**, 1110 (1994); S. Partyka, M. Lindheimer, B. Faucompre, *Colloids Surf. A* **76**, 267 (1993).
18. J. Leimbach, J. Sigg, H. Rupprecht, *Colloids Surf. A* **94**, 1 (1995); T. Gu and Z. Huang, *ibid.* **40**, 71 (1989).
19. These spacings varied somewhat from sample to sample, probably due to surface variations as reported (*7*).
20. T. Gu, B.-Y. Zhu, H. Rupprecht, *Prog. Colloid Polym. Sci.* **88**, 74 (1992).
21. R. M. Pashley and B. W. Ninham, *J. Phys. Chem.* **91**, 2902 (1987).
22. C. A. Helm, J. N. Israelachvili, P. M. McGuiggan, *Science* **246**, 919 (1989).
23. P. Richetti and P. Kekicheff, *Phys. Rev. Lett.* **68**, 1951 (1992).
24. Previous SFA measurements (*21*) with quaternary ammonium surfactants have found that aggregate layers on mica have dissociation constants (20 to 25%) similar to those of spherical micelles. Given that any aggregate curvature should be a function of the dissociation constant (because the degree of charge neutralization affects the interheadgroup spacing), the above measurement is more consistent with curved surface aggregates (such as the proposed cylinders) than with flat bilayers.
25. A. C. Zettlemoyer, *J. Colloid Interface Sci.* **28**, 343 (1968); F. G. Greenwood, G. D. Parfitt, N. H. Picton, D. G. Wharton, in *Adsorption from Aqueous Solutions*, W. J. Weber and E. Matijevic, Eds. (American Chemical Society, Washington, DC, 1968), pp. 135–144.
26. A. M. Koganovskii, *Colloid J. USSR* **24**, 702 (1962).
27. Y. H. Yeo, K. Yackoboski, G. C. McGonigal, D. J. Thompson, *J. Vac. Sci. Technol. A* **10**, 600 (1992); J. P. Rabe and S. Buchholz, *Science* **253**, 424 (1991); A. J. Groszek, *Proc. R. Soc. London Ser. A* **314**, 473 (1970).
28. Control experiments were performed to ensure that the adsorbate morphology was not an imaging artifact: (i) The adsorbate layer on each substrate was imaged in at least three independent experiments with different cantilevers. (ii) The imaged adsorbate morphology was confirmed to be repeatable and independent of scan size, speed, and direction. (iii) In many cases, a single cantilever was used to image two or more different aggregate structures (such as stripes and spheres) on different substrates.
29. A. Kumar, H. A. Biebuyck, G. M. Whitesides, *Langmuir* **10**, 1498 (1994); J. J. McClelland, R. E. Scholten, E. C. Palm, R. J. Celotta, *Science* **262**, 877 (1993).
30. J. M. Schnur, *Science* **262**, 1669 (1993).
31. Q. Huo, R. Leon, P. M. Petroff, G. D. Stucky, *ibid.* **268**, 1324 (1995).
32. W. A. Ducker, T. J. Senden, R. M. Pashley, *Nature* **353**, 239 (1991); H.-J. Butt, *Biophys. J.* **60**, 1438 (1991).

33. We thank H. Rupprecht, S. M. Gruner, V. A. Parsegian, D. E. Walters, and J. P. Cleveland for helpful discussions; W. Heckl for the MoS_2 crystal; and U. G. Hofmann for silica substrates. Supported by a Humboldt Fellowship (S.M.) and the Deutsche Forschungsgemeinschaft (H.E.G.).

6 July 1995; accepted 4 October 1995

Scaling Properties of Stretching Ridges in a Crumpled Elastic Sheet

Alex Lobkovsky, Sharon Gentges, Hao Li,* David Morse, T. A. Witten†

Strong deformation of a sheet of solid material often leads to a crumpled state having sharp points of high curvature. A scaling property governing the crumpled state has been numerically demonstrated by an examination of the ridges joining pairs of sharp points in a range of simple geometries of variable size. As the linear size X increases sufficiently, the deformation energy grows as $X^{1/3}$ and consists of similar amounts of bending and stretching energy. The deformation energy becomes concentrated in a fraction of the sheet that decreases as $X^{-1/3}$. Despite this concentration, the local strain in the ridge decreases as $X^{-2/3}$. Nearly all the deformation energy in thin, crumpled elastic sheets was found to be concentrated in ridges that obey these scaling laws.

Buckled sheets such as a crumpled piece of paper, a collapsed storage tank, or a shriveled raisin represent a ubiquitous form of material deformation. These objects may be considered as thin, elastic sheets that have been strongly deformed by some external force. Such "post-buckling" phenomena have been extensively studied in macroscopic sheets because of their importance for structural failure (*1*, *2*) and for cushioning of mechanical impact (*3*, *4*). Two features emerge from these studies. First, the deformation appears to be concentrated around points and lines that proliferate with increasing compression, as illustrated in Fig. 1. Second, the compressive force increases smoothly over a broad range of compression factors (*3*, *5*). These same features are expect-

A. Lobkovsky, S. Gentges, H. Li, T. A. Witten, James Franck Institute, University of Chicago, Chicago, IL 60637, USA. World Wide Web: http://arnold.uchicago.edu/MRSEC
D. Morse, Institute for Theoretical Physics, University of California, Santa Barbara, CA 93106, USA.

*Present address: NEC Research Institute, Incorporated, 4 Independence Way, Princeton, NJ 08540, USA.
†To whom correspondence should be addressed. E-mail: t-witten@uchicago.edu

ed for microscopic elastic membranes, such as layered compounds (6) (Fig. 1C) and solidlike surfactant vesicles (7).

Current understanding of the strongly buckled state remains primitive. Some scaling properties of this state have been explored empirically (8–10). Still, it is not even known how the energy of a crumpled sheet ought to scale with compression. With such scaling laws one could predict, for instance, the energy of a large crumpled sheet given that of a smaller one. Mathematical treatment of strong buckling has been confined to isolated cases (11–13) in which the buckling behavior is different from that of a crumpled sheet. The bulk of analytical work concerns sheets weakly deformed by thermal fluctuations (14, 15) or by incipient buckling (16, 17). Here, we demonstrate a structural element responsible for the deformation energy of strongly buckled thin sheets: the stretching ridge.

To define this strong buckling, we consider a thin, flat elastic disk confined in an impenetrable sphere. The thickness h of the disk is taken to be much smaller than its radius R_0 so as to accentuate the contrast with an ordinary three-dimensional solid. The confining sphere is gradually contracted to a radius $R < R_0$, so that the elastic sheet within it must deform. A point originally at spatial position $\mathbf{s} \equiv (s_1, s_2, 0)$ moves to the point $\mathbf{r}(\mathbf{s})$. The deformation energy is the sum of the strain energy S and bending energy B. The sheet takes on a conformation $\mathbf{r}(\mathbf{s})$ that minimizes the energy $S + B$.

We expect the confined sheet to bend in preference to stretching when $R \gg h$. Accordingly, we first consider an unstretchable sheet. Every point on such a sheet must have vanishing curvature in some direction (18). If the confining sphere is contracted to two-thirds of the radius R_0, for example, the sheet can distort into a conical shape (Fig. 2A) with a singular curvature at the vertex. At each point of the cone there is no curvature in the direction toward the vertex. The radius of curvature $1/C$ grows linearly with distance from the vertex. The resulting energy $B = \kappa \int^{R_0} d^2s C^2$ grows logarithmically with the size R_0. Here κ is the cylindrical bending modulus, d^2s denotes the surface integration element, and the integration is taken over the surface (16). As the confining sphere is contracted further, a single cone can no longer fit inside it. An increasing number of singular vertices is necessary; hence, we investigated the shape of a surface with two such vertices (Fig. 2B).

The addition of a second vertex alters the curvature qualitatively. A generic point P must now have zero curvature in the direction of both the first vertex and the second. Thus, the surface must be flat except along the line joining the vertices. This line must form a sharp ridge, whose energy is propor-

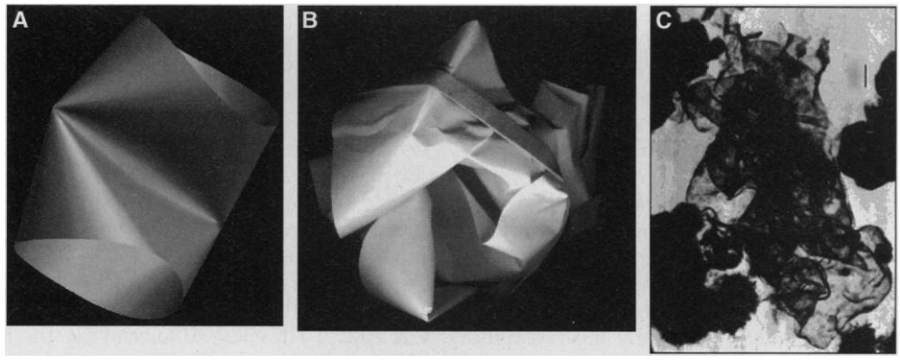

Fig. 1. Examples of buckled and crumpled sheets. (**A**) Simulated buckled thin cylinder [courtesy of the authors of (27)]. (**B**) A piece of paper lightly crumpled between the hands. (**C**) Rag phase of molybdenum disulfide [courtesy of the authors of (28)]. The calibration bar is 20 nm.

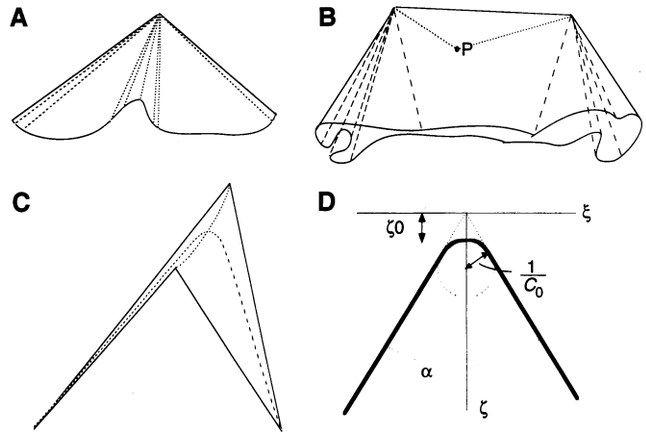

Fig. 2. Deformations of a thin elastic sheet with increasing confinement. (**A**) Cone shape resulting from moderate confinement. (**B**) Double-cone shape resulting from further confinement. A generic point P is indicated. (**C**) Kite shape which exhibits a ridge [such as the one in (B)] being bent through a dihedral angle. (**D**) Approximate shape of the transverse diagonal in (C). Axes for the normal coordinate ζ and the transverse coordinate ξ are shown. Deflection ζ_0 from the unstretchable ridge and dihedral angle α are indicated.

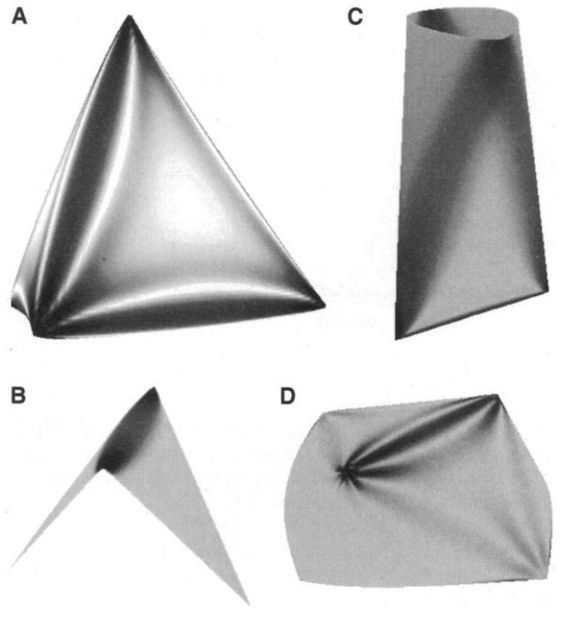

Fig. 3. Sample shapes simulated with a triangular lattice of springs of unstretched length a and spring constant K. Shading is proportional to the local stretching energy. Bending rigidity is imparted by an additional energy $J(1 - \hat{n}_i \cdot \hat{n}_j)$ for each pair of adjacent triangles (i, j) with unit normals $\hat{n}_i$ and $\hat{n}_j$ (13), where J is proportional to the bending modulus. This lattice is equivalent to a sheet of isotropic elastic material of thickness $h = 2\sqrt{2}\sqrt{J/K}$ and bending modulus $\kappa = J\sqrt{3}/2$. (**A**) Regular tetrahedron. The distance X between vertices is 100 times the lattice spacing a. Elastic thickness $h = a/27.4$. (**B**) Kite shape made from a flat, rhombus-shaped surface by exerting normal forces on the perimeter sites. The forces constrain the perimeter to follow a rectilinear frame with a dihedral angle α equal to that of the tetrahedron, namely $\cos^{-1}(1/3)$. Ridge length $X = 100a$ and thickness $h = a/13.7$. (**C**) Two-vertex bag shape with $X = 50a$, $h = a/27.4$, and length of $2X$. The "sharpness" of the vertices (integrated Gaussian curvature or disclination charge) is π, as in a regular tetrahedron. (**D**) Two-vertex boat shape with $X = 67.48a$ and $h = a/20.4$. The two vertices have sharpness $\pi/3$.

tional to its length. The energy increases with the system size R_0 qualitatively more rapidly with two vertices than with one. If the surface is allowed to stretch, the effect on the single cone is minor: the singularity at the vertex spreads over a finite region whose size is independent of R_0. In the case of two vertices [discussed elsewhere (*19*)], it has been argued that stretching allows the ridge to soften to a radius of curvature 1/C of order $h^{1/3} R_0^{1/3}$. The associated energy was argued to grow as $R_0^{1/3}$. For very thin sheets, such an energy would be qualitatively larger than the single-vertex energy, yet qualitatively smaller than the energy of an unstretchable sheet.

We may extend the energy-balance reasoning (*19*) to treat the ridge joining two vertices, as in the double-cone shape of Fig. 2B. We consider an initial state in which the stretching moduli G are very large and the ridge is a sharp crease of length X, bent through a dihedral angle α, like the kite shape of Fig. 2C (*20*). The moduli G are gradually decreased so that stretching is allowed and the transverse curvature at the ridge relaxes, assuming a value C_0 at mid-ridge. We suppose, and later justify, that the bulk of the deformation occurs in a strip along the ridge of width $w \simeq 1/C_0$. Then, as C_0 decreases, the strip must deflect away from the original ridge line by an amount ζ_0 of order $1/C_0$. (If the transverse lines were simply rounded at the apex as shown in Fig. 2D, then $\zeta_0 = \{[\sin(\alpha/2)]^{-1} - 1\}/C_0$.) The deflection of the strip results in stretching along the ridge: the sheet must be strained by an amount $\gamma \simeq (\zeta_0/X)^2 \simeq (XC_0)^{-2}$. The energy $S = G \int d^2s\gamma^2$ for this stretching of the strip is of order $G\gamma^2 Xw \simeq GX^{-3}C_0^{-5}$. The energy B to bend the strip is of order $\kappa C_0^2 Xw \simeq \kappa XC_0$. To minimize the sum of these two energies requires $C_0 \simeq (1/X)\,[X/(\kappa/G)^{1/2}]^{1/3}$. For sheets made of isotropic material, the length $(\kappa/G)^{1/2}$ is approximately equal to the thickness h (*16*). The optimal energy achieved is of order $S \simeq B \simeq \kappa(X/h)^{1/3}$.

To reduce the ridge energy further would require deformation in other regions, but the cost of such deformations would outweigh their benefit. Thus, to reduce the distance X between the vertices substantially would require a strain of order γ over much of the surface—a region much larger than the ridge. The energy cost would clearly be larger than the ridge energy. Likewise, if the flanks of the ridge stretched so as to reduce the needed deflection of the ridge line, the required strain would be of order γ over much of the surface, and the cost would again be prohibitive.

To test these scaling predictions, we modeled the elastic sheet numerically as a triangular lattice of springs, following, for example, Seung and Nelson (*13*, *21*, *22*). Some minimum-energy surfaces having a variety of secondary structures near each ridge are shown in Fig. 3. The stretching energy oscillates as one moves away from the ridge line of the tetrahedron rather than going monotonically to zero. For the shapes with a free edge (Fig. 3, C and D), there are regions of large curvature at the free edge opposite to the vertices. Faint induced ridges appear between the vertices and the induced "vertices" at the edges. These induced features become stronger as the effective size X/h increases.

We plotted the transverse curvature at mid-ridge versus the reduced size X/h for the four different shapes (Fig. 4). The curvature is expressed relative to the curvature at the same point if only one vertex were present. We note first that the curvatures follow the anticipated $(X/h)^{1/3}$ scaling. The tetrahedron has a reduced curvature of $0.22(X/h)^{1/3}$, as determined from fitting all the data. The uncertainty in this coefficient derived from the scatter of the data is less than 0.001. Second, the curves for different shapes have similar slopes. This indicates that the shape of the ridge does not depend strongly on the sharpness of the vertices or on the shape of the surface far from the ridge. Third, the dihedral angle α affects the slope more than the sharpness of the vertices does. For the bag shapes (Fig. 3C) with fixed sharpness, the slope increases with the bag length (that is, with decreasing α), but for different shapes with equal dihedral angles (Fig. 3, A and B), there is no discernable difference in slope. Fourth, in all cases, the ridge begins to dominate the curvature (doubling the reduced curvature) for X/h in the range of 350 to 1000.

We analyzed the tetrahedral shape in greater detail. We first verified that the shapes were independent of lattice size for fixed X/h. The curvature at mid-ridge differs from the extrapolation to an infinitely fine lattice by no more than 2%. The entire profile shrinks inward with increasing X/h; the shrinkage is consistent with the anticipated $(X/h)^{-1/3}$ scaling. This can be seen by plotting the mean squared curvature across the ridge as shown in Fig. 4B for four different values of X/h. The ridge profiles collapse onto a single scaling curve. Because our results are insensitive to the lattice spacing for a given X/h, they are not sensitive to the lattice spring model used, but they would hold quantitatively for any elastic material.

The total energy of the tetrahedron is expected to scale as $\kappa(X/h)^{1/3}$. The measured total energy $S + B$ in units of κ is plotted in Fig. 5. The energy is consistent with the asymptotic formula $S + B = 6\kappa(1.55 \pm 0.002)\,(X/h)^{1/3}$. The indicated uncertainty reflects only the scatter in the data used. For comparison the combined energy of the four disconnected cones making up the tetrahedron is shown; namely,

$$4\kappa[4.081 \log(X/a) + \text{constant}] \quad (1)$$

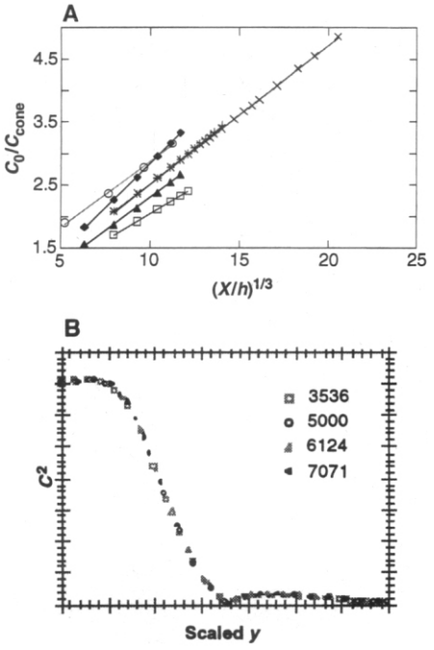

Fig. 4. (**A**) Mid-ridge curvatures for simulated surfaces relative to the curvature of a single cone at the same distance from its vertex. The horizontal axis is the anticipated scaling variable $(X/h)^{1/3}$. Open squares, kite shapes; open circles, boat shapes; closed triangles, bags of length X; closed diamonds, bags of length $2X$; black plusses, tetrahedrons with ridge length $X = 50a$; gray x's, tetrahedrons with ridge length $X = 100a$. Straight lines indicate the anticipated scaling behavior. (**B**) Mean squared local curvature C^2 scaled by $X^{-2}(X/h)^{2/3}$ along the perpendicular bisector of the ridge. The distance y from the ridge is scaled by $X(X/h)^{-1/3}$ for tetrahedron ridges with different X/h as indicated. The strain profile $\gamma(y)$ is similar.

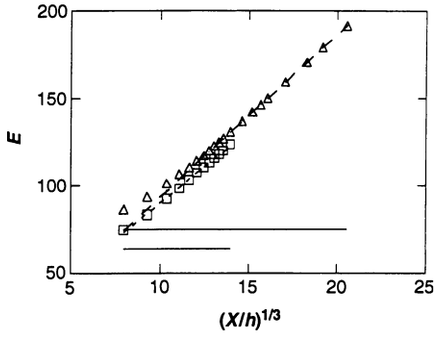

Fig. 5. Total energy $E = S + B$ in units of bending modulus κ for lattice tetrahedra with $X = 50$ lattice units (squares) or 100 lattice units (triangles), versus $(X/h)^{1/3}$. The dashed lines indicate the least square fits through the upper seven points of the data. The solid lines indicate the continuum energies of four separated cones with sharpness π as in a tetrahedron and with length X, determined from Eq. 1 without the additive constant: lower line, $X = 50$ lattice units; upper line, $X = 100$ lattice units (numerically determined cone energies fall close to these lines).

The cone energy is independent of the moduli G and thus independent of the elastic thickness h (*23*). The cone energy remains a significant fraction of the tetrahedron energy for all tetrahedra studied. Nevertheless, the asymptotic scaling gives less than 10% error for tetrahedra larger than about 10^3 times their thickness (for example, a 10-cm tetrahedron made of standard 0.1-mm-thick office paper). The simulated sheets of Tersoff (*24*) and of Kroll (*22*) did not approach these size-to-thickness ratios; thus, it is not surprising that they saw no evidence for the energy scaling predicted here.

The ridges suggest an approach for describing a strongly crumpled sheet. From common observation, crumpled sheets contain a large number of vertices. We may suppose that pairs of adjacent vertices give rise to ridges like the ones seen in our simple shapes. The neighboring ridges can be expected to influence one another. Still, this mutual influence cannot be too great. Our study has shown that well-developed ridges are but little influenced by the surface at distances of order X from the ridge line. This is natural, because the ridge energy is concentrated at distances much smaller than X from this line. We are led to treat the ridges as independent, at least as a first approximation. Thus, we may find the approximate energy of a given crumpled sheet from its ridge lengths X_i by simply adding the individual energies to obtain a total energy $E \approx \kappa \Sigma_i (X_i/h)^{1/3}$.

We expect the stretching-ridge concept to contribute to future understanding of the crumpled materials like those in Fig. 1. When the ridges are a few hundred times longer than the membrane thickness, they give a quantitative account of the deformation energy. The ridge concept should aid in the design of macroscopic energy-absorbing materials such as packing material (*4*) and protective vehicle structures (*3*), for example, by placing defects to control where ridges form. Knowledge about ridges may aid the understanding of microscopic phenomena such as the collapse of graphite membranes (*6*) and the passage of blood cells through capillaries (*25*), and it may elucidate large-scale phenomena such as the buckling of the Earth's crust (*26*).

REFERENCES AND NOTES

1. *Post-Buckling of Elastic Structures*, proceedings of the *Euromech Colloquium*, no. 200, Matrafured, Hungary, 5 to 7 October 1985 (Elsevier, Amsterdam, 1986).
2. N. Yamaki, *Elastic Stability of Circular Cylindrical Shells* (North-Holland, New York, 1984).
3. P. Stutenkemper and R. Brasche, in *International Technical Conference on Experimental Safety Vehicles*, sponsored by the Government of France, Paris, 5 to 8 June 1979 (Government Printing Office, Washington, DC, 1980), pp. 321–329.
4. C. E. Crede, in *Symposium on Simulated Service Testing of Packaging*, Sponsored by the Administrative Committee on Simulated Service Testing, New York, NY, 1962 (American Society for Testing and Materials, Philadelphia, PA, 1963), pp. 1–49.
5. R. E. Newton, in *Shock and Vibration Handbook*, C. M. Harris and C. E. Crede, Eds. (McGraw-Hill, New York, 1988), p. 31-1; P. E. Franklin and M. T. Hatae, *ibid.*, p. 41-1.
6. M. S. Spector, E. Naranjo, S. Chiruvolu, J. A. Zasadzinski, *Phys. Rev. Lett.* **73**, 2867 (1994).
7. E. Sackmann *et al.*, *Ber. Bunsen-ges. Phys. Chem.* **89**, 1198 (1985).
8. J. B. C. García, M. A. F. Gomes, T. I. Jyh, T. I. Ren, *J. Phys. A. Gen. Phys.* **25**, L353 (1992).
9. F. Abraham, paper presented at the Workshop on Biomaterials, University of California, Santa Barbara, CA, 31 August 1994.
10. Y. Kantor, M. Kardar, D. R. Nelson, *Phys. Rev. Lett.* **57**, 791 (1986).
11. R. Scheidl and H. Troger, in (*1*), p. 293.
12. M. Ortiz and G. Giola, *J. Mech. Phys. Solids* **41**, 531 (1994).
13. H. S. Seung and D. R. Nelson, *Phys. Rev. A* **38**, 1005 (1988).
14. D. Nelson, T. Piran, S. Weinberg, Eds., *Statistical Mechanics of Membranes and Surfaces* (World Scientific, Singapore, 1989).
15. D. R. Nelson and L. Peliti, *J. Phys. (Paris)* **48**, 1085 (1987); F. David and E. Guitter, *Europhys. Lett.* **5**, 709 (1988).
16. L. D. Landau and E. M. Lifshitz, *Theory of Elasticity* (Pergamon, Oxford, 1986), sections 14 and 15. Our cylindrical bending modulus κ is denoted there as D.
17. See, for example, G. Gerard, *Handbook of Structural Stability* (New York University, New York, NY, 1956).
18. In (*14*), p. 143.
19. T. A. Witten and H. Li, *Europhys. Lett.* **23**, 51 (1993).
20. A full description requires two stretching and two bending moduli; however, these details are not important for our scaling argument.
21. D. C. Morse and T. C. Lubensky, *J. Phys. II* **3**, 531 (1993).
22. Z. Zhang, H. T. Davis, D. M. Kroll, *Z. Phys. B* **97**, 337 (1995).
23. More precisely, the cone energy is independent of h in the limit that h is much smaller than the lattice spacing a. In our numerical studies h varied from a to a few percent of a. Accordingly, we observed a few-percent dependence of the cone energy on h.
24. J. Tersoff, *Phys. Rev. B* **46**, 15546 (1992).
25. W. H. Reinhart *et al.*, *Biorheology* **28**, 537 (1991).
26. See, for example, R. J. Chorley, S. A. Schumm, D. E. Sugden, *Geomorphology* (Methuen, London, 1984), chap. 7.
27. Y. L. Kergosien, H. Gotoda, T. L. Kunii, *IEEE Comput. Graphics Appl.* **14**, 40 (1994).
28. R. R. Chianelli, E. B. Prestridge, T. A. Pecoraro, J. P. DeNeufville, *Science* **203**, 1105 (1979).

29. We are grateful to J. Gao, N. Lebovitz, S. Antman, and S. Nagel for assistance and discussions. Supported by NSF under award number DMR-9205827 and through its Materials Research Science and Engineering Center Program under award number DMR-9400379. S.G. was supported as a summer intern by the NSF Research Experiences for Undergraduate Program under NSF Research Experience for Undergraduates site grant Phy-9212351. We thank the authors of (*27*) for providing the image for Fig. 1A.

3 July 1995; accepted 29 September 1995

Autoencapsulation Through Intermolecular Forces: A Synthetic Self-Assembling Spherical Complex

Robert S. Meissner, Julius Rebek Jr.,* Javier de Mendoza

The synthesis and characterization of a system for the study of molecular recognition phenomena are described. The system involves a tetraurea molecule that is capable of assembly into various associated states through hydrogen bonding. In organic solvents, the dynamic transition between a low-ordered (aggregate) state and a highly ordered dimeric assembly can be induced by the introduction of smaller molecules of appropriate size and shape. These smaller molecules, such as benzene, adamantanes, and ferrocenes, act as guests that occupy the pseudospherical capsule formed by the dimeric host. Among various guests, those that best fill the cavity and offer chemical complementarity to the host are preferentially encapsulated.

How molecules fit together—molecular recognition—can be explored with biological macromolecules and with synthetic structures of low molecular weight. Recognition expresses structural information and takes the form of complementarity in size, shape, and chemical surfaces. A subtle expression of information is possible with self-complementary molecules. Multiple copies of such molecules can give rise to ordered superstructures—assemblies—with functions that are unique to their assembled states. In molecular assembly formation, favorable binding forces (enthalpy) compete with energy loss due to the decreased freedom of the individual subunits (entropy). Guest molecules that match a host assembly in size and shape interact to produce an increased van der Waals attraction, and those guests with functional groups capable of forming hydrogen bonds with the host produce increased electrostatic attraction. Guests that maximize the attractive forces are preferred (*1*). Here we describe a molecule that assembles to provide a host for the reversible encapsulation of sizable, complementary guests (*2*).

Molecule **1** consists of 13 fused rings that

R. S. Meissner and J. Rebek Jr., Massachusetts Institute of Technology, Department of Chemistry, Cambridge, MA 02139, USA.
J. de Mendoza, Universidad Autonoma de Madrid, Departamento de Quimica, Cantoblanco, 28049 Madrid, Spain.

*To whom correspondence should be addressed.